Dalton Transactions

ROYAL SOCIETY OF CHEMISTRY

PAPER

View Article Online
View Journal

Cite this: DOI: 10.1039/d6dt01004k

The quest for electrokinetic control over bulk zeolite synthesis: trials, challenges and effects

Mostafa Torka Beydokhti, † Gleb Ivanushkin † and Michiel Dusselier *

While electrostatic stabilization between negatively charged aluminosilicate species and positively charged structure-directing agents is widely recognized as a key driving force in zeolite crystallization, the net interaction energy is often a superposition of Coulomb, steric, van der Waals, and solvation contributions, which are challenging to deconvolute experimentally. Close energetic competitions and metastability often prioritize kinetic control over thermodynamic stability, which cannot always be described by classical kinetic laws. Here, taking into account the charge-rich media, we hypothesize that electrokinetic control (EKC) can be considered as a reactor-based adaptation for manipulating the crystallization of microporous materials, as was illustrated in the state-of-the-art for proteins. Various crystallizing zeolite systems were experimentally studied under (high-)voltage direct and alternating current (DC and AC) electric fields (EFs) up to 20 kV, using different reactor setups. The conceptual ideas of EKC effects in steering zeolite nucleation and crystallization thermodynamics and kinetics were tested. The potential effects of EKC over hydrothermal synthesis were assessed through product phase selectivity, particle size, and aluminum content. Four different setups were developed to match the studied EF modes (internal and external, with both uniform and non-uniform fields). The setup designs and EF configurations were further complicated by the need to adapt them to the harsh conditions of bulk hydrothermal synthesis. We believe this work offers valuable insights into the effects of charge interactions during intricate zeolite synthesis. While inconclusive in many series of experiments, this experimental work details the journey of our search for EKC across a wide range of conditions. Its results, supported by conceptual theories, can guide future researchers in how to select appropriate EF parameters, build effective reactor setups, and target the right types of zeolite recipes to maximize the chances for manipulating zeolite nucleation and growth using EKC.

Received 29th April 2026,
Accepted 19th May 2026

DOI: 10.1039/d6dt01004k

rsc.li/dalton

1. Introduction

Conventional hydrothermal synthesis often lacks precise control over reaction conditions, which can limit phase purity and restrict the accessible range of compositions (*e.g.*, Si/Al ratios) and zeotype diversity.[1] This restriction can also be framework-driven. In addition to chemical modifications applied to conventional hydrothermal synthesis precursor preparation, reactor-based innovations have increasingly gained prominence,[2] trying to address the aforementioned lack of controls or looking to introduce energy in alternative ways. It is often assumed that the primary barriers to zeolite formation are of kinetic nature, since all zeolite frameworks are energetically favorable and metastable with respect to the most thermodynamically stable siliceous phase – quartz.[3] The formation enthalpy of hydrated zeolites is favorable, which compensates for their unfavorable metastability relative to quartz. However, the formation entropy of hydrated zeolites is unfavorable. The combined negative enthalpy and negative entropy cause the Gibbs free energy to vary even less between different frameworks.[3]

Electrokinetic control (EKC) of crystallization is primarily considered as a kinetic process, as it involves the (temporal) manipulation of charged species dynamics (*i.e.*, motion) under an applied electric field (EF). However, electrokinetic effects can also influence the thermodynamics of nucleation through supersaturation and modify the interfacial energies of crystals during growth.[4] EKC has been previously explored in protein crystallization,[4–13] with increasingly refined theories describing its thermodynamic and kinetic effects on nucleation and growth. Initially, the theory was applied to nucleation in uniform vapor–liquid systems (*e.g.*, water condensation);[14] these approaches have been expanded to non-uniform liquid–solid systems.[4,15–17] Moreover, charge transport under EF, particularly through (di-)electrophoretic forces, has also been investigated in the context of phase separation-induced crystal-

Center for Sustainable Catalysis and Engineering (CSCE), KU Leuven, B-3001 Leuven, Belgium. E-mail: michiel.dusselier@kuleuven.be
† M. T. B. and G. I. contributed equally.

lization.[18] Theoretically, an external (meaning non-contacted with the media) EF can influence the thermodynamic properties of a system, such as chemical potential, Gibbs free energy, and Helmholtz energy, introducing additional parameters for control.[4] The change in chemical potential between the solid and liquid phases depends on the difference in their dielectric permittivity, which can either lower or raise the nucleation energy barrier, thereby modulating the nucleation rate.[4,19] In this context, both direct current (DC) and alternating current (AC) high-voltage EFs can be employed to alter the dielectric environment of the nucleating phase. The extent of nucleation enhancement is governed by the field strength, frequency (in the case of AC), and the intrinsic electrical properties of both the solvent and the crystallizing species.[4,16] Internal EF is where the electrodes are in direct contact with the medium, which can thus also include electrochemistry. Although EKCs are often categorized separately from electrochemistry, they can encompass electrochemical phenomena through mechanisms, such as charged particle migration, triggering local supersaturation, and perturbation of the electrical double layer (EDL), especially when the potential–current window is confined to capacitive regions, limiting faradaic reactions.[6,9] Mainly, the EKC effects on crystallization include reduction/enhancement of the nucleation rate, spatial control over nucleation sites, crystal size control, decrease/increase of yield, crystal orientation control, quality of crystals (*e.g.*, by reducing defects through increased step's free energy on crystal facets[4]) and control over polymorphism.[4,7–9,13]

To this date, in the field of microporous materials, EFs have been applied in zeolite bulk crystallization (our own work),[20–23] film deposition,[24–27] and post-synthesis treatment.[28,29] There are also multiple examples of utilizing EFs of different nature in MOF synthesis;[30,31] however, we would refer the reader to a comprehensive review on this subject since this class of materials is out of scope here.[32] Except for the post-synthesis treatment, where the EF is applied directly to pre-made zeolite powders, these applications have primarily involved internal EFs with clear electrochemistry, either during bulk crystallization,[20–22] at the electrode/substrate interface,[25–27] or during the deposition of as-synthesized zeolite films.[33–36] There is also a recent review on the film deposition of zeolitic materials (including zeolites and MOFs) and their applications in electrochemical energy conversion and storage.[37] High-voltage EF (up to 8×10^5 V m^{-1})[28,29] has been explored as a pre-activation step to modify the gas adsorption and separation behavior of zeolites. The flexibility[38] of T–O bonds, T–O–T angles, and extra-framework cations was thought to make them susceptible to vibration and displacement under high-strength EFs, which could therefore modulate the crystal structure by altering accessibility and porosity.[39] On the other hand, as-synthesized zeolite film deposition leverages the intrinsically charged nature of the crystals that arises from surface silanol groups, alumina sites, and related defects, driving particles toward the deposition electrode or substrate. The configuration of the deposition setup, EF strength and electrode arrangement governs the interactions and movements of charges and charged particles (*i.e.*, electrostatic interactions, such as coulombic forces, (di-)electrophoresis and dipole–dipole interactions), which represent the dominant electrokinetic influences in this context.[40] In the case of *in situ* crystallization, whether occurring in the bulk material or at the electrode/substrate interface, electrochemical reactions play a significant role. Nevertheless, during film deposition on a substrate, the transport and diffusion of reactants, along with the resulting increase in local supersaturation, can still be the dominant driving forces. In the case of bulk synthesis, our group developed an *in situ* electrochemical cell for the dedicated synthesis of zeotypes in bulk solution.[22] Potentiostatic anodic dissolution enables the controlled, timed addition of metals, effectively overcoming the limitations associated with conventional heteroatom precursors, particularly during nucleation, and enhancing element incorporation efficiency. Recently, another research group applied microplasma electrochemistry for zeolite bulk synthesis.[23] However, in this specific case, the role of electrochemistry remains somewhat ambiguous, as the primary influence appears to stem from hydroxyl radicals generated by the microplasma itself. These radicals seem to accelerate crystallization and modulate crystal properties.[41]

In this paper, we explain some of the limitations in bulk zeolite synthesis and test our hypotheses for addressing these by applying EF over a range of hydrothermal bulk syntheses. By applying EFs of significant magnitude, we would expect that the non-classic kinetics for different phases (topology) and stages, or even Al density, can be changed to different degrees, thus impacting zeolite synthesis selectivity. In general, we will probe the existence of EKC in zeolite synthesis and hypothesize 3 different modes of kinetic disturbance: (i) introduced non-random, additional mobility of charged species in the bulk; (ii) the influence on critical events of zeolite crystallization (mainly impacting nucleation); and (iii) high-field strengths disturbing Coulomb interactions (*e.g.*, shielding and EDL). In this regard, we present our trials on high-voltage external and internal EFs (also under a wide range of frequencies) for probing our rationales. The use of (high-)voltage external/internal EFs has never been explored to assess the nucleation and crystallization of zeolites in the bulk. Several reactor configurations have been developed for applying these fields, with their respective challenges and limitations also being addressed. Different zeolite synthesis systems are selected to estimate the impact of EFs on diverse types of synthesis and crystallization mixtures and different topologies (phases). The possible influences of EFs were investigated through material properties as witnessed in PXRD (phase), ICP-AES (elemental composition) and SEM analysis (morphology, size). Finally, we conclude on the effectiveness and feasibility of EF effects on zeolite crystallization, based on our findings, initial hypotheses and the literature, and provide directions to guide future researchers.

2. Experimental section

2.1. Synthesis of zeolites and EKC

The synthesis methods were adapted from ref. 42–52 listed in Table S1 and provided in the SI. After preparing the synthesis mixture, it was evenly divided into portions for batch, 0 V = silent (if applicable), and EKC conditions (x V_{PP} where x is the voltage). So, a batch means the vial/vessel with no electrode, 0 V(silent) means the vessels with electrodes inside without an applied EF, and EKC means the synthesis with the applied EF over the electrodes, while a conventional batch means the Teflon-lined stainless steel autoclave. Once the oil bath reached the target temperature (monitored *via* a thermocouple placed inside the oil, or in a batch), the reactors were immersed and maintained at that temperature for a specified duration. Upon completion of the synthesis, the reactors were quenched in a water bath at room temperature for 15 min and then the mixtures were centrifuged at 6700–11 000 rpm for an appropriate time. The supernatant was discarded (if not subjected to elemental analysis), and the remaining solid was resuspended in deionized water, shaken, and centrifuged. This washing process was repeated at least three times until the pH of the discarded liquid dropped below 9. Finally, the solid product was dried at 60 °C for 24 hours.

For the wide frequency screening, a "characteristic frequency" value was selected from the calculations based on LCR-meter measurements using the following formula:

$$f_{\text{char}} = \frac{\omega_{\text{char}}}{2\pi} = \frac{1}{2\pi\sqrt{L \times C}}$$

where L is the inductance and C is the capacitance of the media. Theoretically, a closed $LC(R)$ circuit (containing an inductor, a capacitor and a resistor) forms a harmonic oscillator, which has the ability to resonate depending on its impedance with a characteristic frequency. Commonly, the values of L and C were measured from the prepared liquid precursors mixture, right before the synthesis protocol (*i.e.*, heating of the initial gel) was initiated. Besides the EAB precursor mixture (2 separate measurements), CHA and MFI prepared solutions (conditions – Table S1, entries 9 and 10) were tested, which gave 902 and 844 Hz, respectively.

2.2. Characterization techniques

The structure phase and crystallinity of materials were examined with powder X-ray diffraction (PXRD) using a high-throughput STOE STADI P Combi diffractometer in the transmission mode equipped with Ge(111) monochromatic X-ray inlet beams (λ = 1.5406 Å, Cu Kα source). The scanning time for the powder of each sample was 10 min. The elemental analysis, inductively coupled plasma-atomic emission spectrometry (ICP-AES), was conducted on a PerkinElmer Optima 3300 DV machine with signals for Si, Al and Co at 251.6, 238.2 and 228.6 nm, respectively. Before the analysis, the samples were dissolved in HF. In this respect, 10 mg of samples, 0.24 ml of aqua regia (3 : 1 volumetric mixture of HCl (37%) and HNO_3 (65%)) and 0.42 ml of HF (40%) were poured respectively into a 20 ml polypropylene bottle. After 3 h of dissolution, 5 ml of a 30 g l^{-1} solution of boric acid was added to neutralize the mixture, followed by increasing the volume to 20 ml using deionized water. Finally, for measurement, the samples were diluted with 0.42 M of HNO_3 solution by a factor of 20. **Caution:** Handling concentrated HF solutions requires strict safety measures and should only be undertaken by trained personnel. The structure of the samples was investigated by scanning electron microscopy (SEM) on a Jeol JSM-6010LV microscope at an acceleration voltage of 5–20 kV. A thin layer of the samples' powder was stuck on a piece of carbon tape, on which an electron-conducting Pd/Au (60/40 ratio) film was deposited.

3. Results and discussion

3.1. Hypothetical control over zeolite crystallization by electrokinetic means: myth or reality?

A zeolite crystallization process is governed by complex kinetic barriers and thermodynamic driving forces.[3] Achieving the desired zeolite phases often relies on trial and error rather than on a fully controllable host–guest synthesis process, particularly when using organic structure-directing agents (OSDAs) with poorly understood transient inorganic–organic interactions. A specific topology defined by its T-atom distribution and composition may be energetically less favorable (metastable outcome A, Fig. 1A), yet it can still form when the energy barrier to a more stable phase is sufficiently high (metastable outcome B, Fig. 1A). As such, it is possible to isolate the desired metastable phases by suppressing the subsequent formation of more thermodynamically favorable structures. This enables access to novel (meta)stable phases in terms of both composition, such as heteroatom content and zeotype identity, and framework structure.

Kinetic outcomes in zeolite synthesis cannot be fully explained by classical kinetic parameters, such as temperature (*via* Arrhenius dependence) or reagent concentration and orders, despite their influence on reaction rates. This lack of control is due to the interplay between different stages (pre-ordered, ordered, nucleation, growth and consumption) of different competing phases and/or T-atom outcomes (distribution, content), on top of liquid–solid influences, all with different rate-determining steps and simultaneous occurrence. Thus, additional factors, beyond these classic kinetic parameters, play a dominant role in determining barriers during zeolite synthesis, particularly those arising from the poorly understood interactions within the "black box" of crystallization. These interactions can be divided into: (1) Coulomb electrostatic interactions between myriad charges in synthetic media (Fig. 1B, inorganic cations (*e.g.*, (in)organic structure-directing agents, (in)OSDA, anionic counter ions, silica and alumina monomers); (2) species interactions from pre-ordered to ordered stages such as oligomers, building units, nanoparts and crystals (Fig. 1C and D); and (3) local concentration gradients and supersaturation, which is linked with solubility,

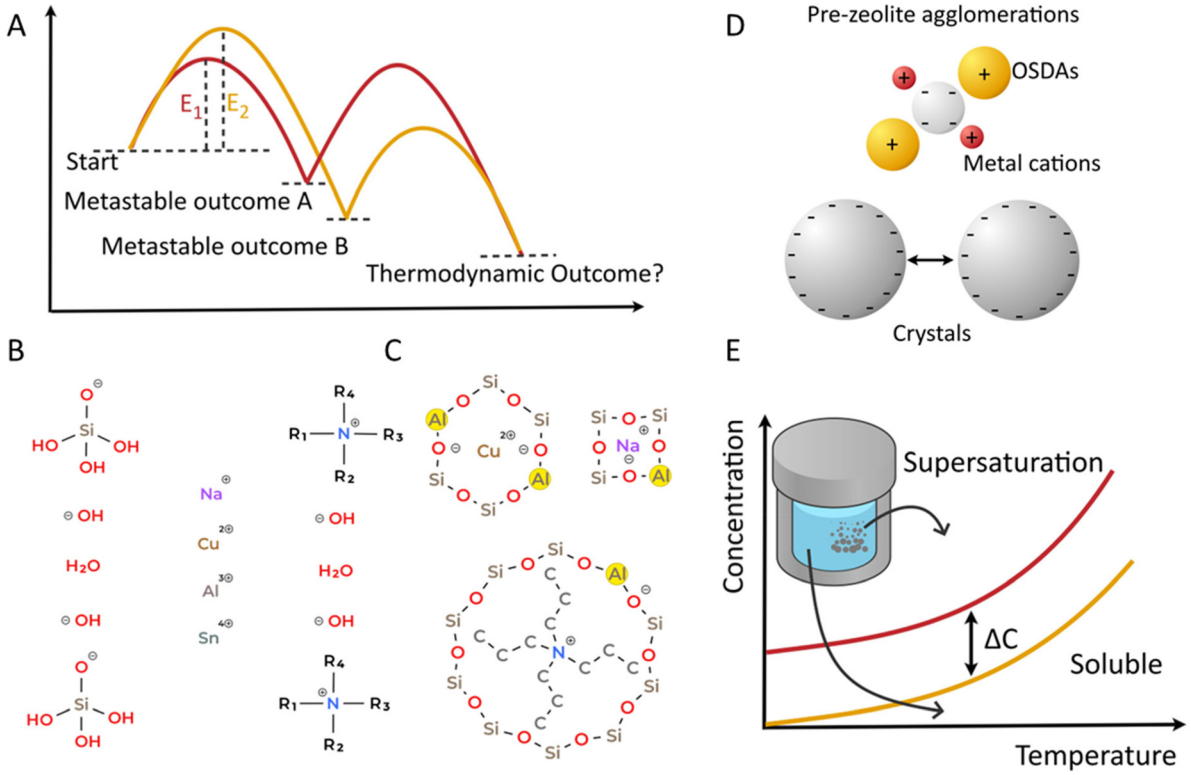

Fig. 1 (A) Reaction coordinate diagram of zeolite synthesis with competing kinetic metastable outcomes. Thermodynamic outcomes are not frequent in Al- and OSDA-containing OH^- syntheses, nor is classic kinetic control. A complex interplay of factors impacts kinetics. (B) Myriad of charged entities in the starting synthesis mixture; many of these cations are not naked but surrounded by a hydration sphere. (C) Charged species in the pre-ordered stage of synthesis. (D) Interaction of charged pre-zeolite agglomerations and (proto)crystals in the pre-ordered and ordered stages of synthesis. (E) Supersaturation and soluble zones in the crystallization process.

mobility, consumption and sedimentation of species impacting nucleation and growth (Fig. 1E).

The role of charge interactions even between, for example, $OSDAs^+$ and many other charged species, such as OH^-, $H_3SiO_4^-$ and (extra)framework $H_3AlO_4^-$ species, M^+, in the crystallization kinetics and thus zeolite product outcomes is largely unknown. Our goal is to employ EF as a reactor-based modification to conventional zeolite synthesis, aiming to manipulate all these mentioned interactions. The role of EKC in zeolite crystallization was analyzed, particularly in terms of its expected impact on crystallization behavior. The effects can be attributed to changes in nucleation, leading to phase selectivity and particle size variation. Also, charge movement and manipulation of Coulomb interactions among different species can result in changes in heteroatom distribution, phase selectivity, and local supersaturation induction. A wide range of synthesis conditions (both dilute and concentrated), including interzeolite conversion (IZC)[53] and charge density mismatch (CDM),[54] were chosen to investigate the effects of EKC on crystallization. It is particularly fascinating how these two synthesis approaches have emerged as unconventional strategies in zeolite synthesis over the past two decades, enabling manipulation of key interactions during the crystallization process. Starting with a crystalline framework as the T-atom source (silica, alumina, and/or heteroatoms), IZC enables adjustment of the local charge ratio (charge of dissolved aluminosilicates) while maintaining a constant overall concentration. The distinctive behavior of a parent crystalline zeolite dissolution is governed by the framework type, composition, and nature and concentration of other ingredients, which offers a tool to control the charge density of the resulting dissolved nanoparticles *versus* (in)OSDA and introduce localized supersaturation zones.[53] On the other hand, CDM leverages different charge densities of polymerized aluminosilicate species (also for heteroatom-containing aluminophosphate),[55] to induce the nucleation of specific frameworks, depending on OH^-, AlO_2^- and OSDA concentrations.[48,54,56]

3.2. Technical reactor configurations and EF modes

One of the key challenges in EKC-based zeolite synthesis lies in designing a reactor that can withstand the extreme hydrothermal conditions, which significantly constrain feasible configurations by high temperature, medium pressures, alkalinity, presence of fluorine anions, *etc*. Moreover, applying a high-voltage EF to a Teflon-lined stainless steel autoclave not only raises significant safety concerns due to the electrical hazards, but also increases sealing challenges. A short circuit caused by inadequate electrical insulation at the electrode terminals can

neutralize the applied EF, undermining the process or causing electrocution. In this scope, and based on our previous experience with designing a reactor for electro-assisted zeolite synthesis, we rely on selective trial and error and the occasional short-circuiting of the lab.[22] The final version of the anodic dissolution reactor features a custom Teflon-made head space, which insulates the whole system. We have used this reactor and other designs in this study.

Here, we classify on the basis of internal/external, AC/DC, and also nonuniform/uniform fields, with different design limitations and safety concerns. An internal EF configuration inherently produces nonuniform fields, particularly with rod-like electrodes, while plate-like electrodes often fail to generate a uniform field across the entire bulk volume of the synthesis mixture.[57,58] Installing an external EF over a conventional reactor is even more critical, as inserting the plate electrodes within or outside the reactor walls is impractical. This constraint often necessitates the use of a cubic reactor design. Applying an internal EF, where electrodes are in direct contact with the solution on the other hand allows for water electrolysis to occur, generating hydrogen and oxygen gases, which increases pressures and alters reaction conditions (faradaic *vs.* capacitive) and concentrations.[22] Internal EF demands precise control of voltage and current within a narrow operational window, making this mode suitable for AC field studies[9] (and preferably in the high-frequency range).

Different modes and configurations of the system used for EKC over bulk zeolite synthesis are illustrated in Fig. 2. The low-voltage DC and AC fields were applied using a waveform generator (GW Instek MFG-2230), which could be ancillary followed by a linear amplifier (FLC Electronic AB; for DC, the output frequency was 1 μHz so that each half-cycle takes 5.8 days). On its own, the waveform generator is capable of producing EFs with voltages up to ±20 V_{PP} at frequencies as high as

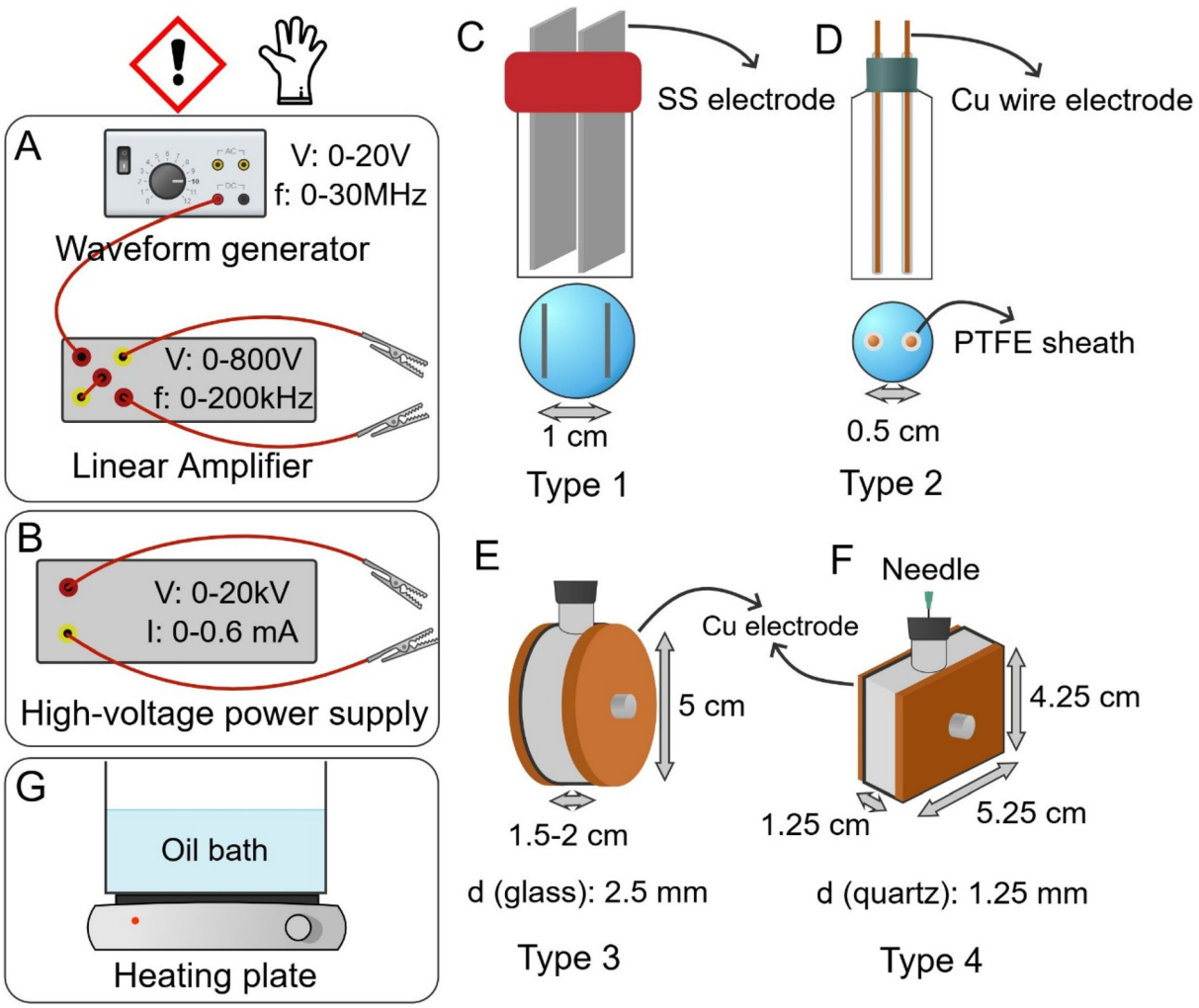

Fig. 2 Reaction setups for EKC over zeolite synthesis: (A) waveform generator for the AC/DC field up to ±20 V_{PP} followed by a configuration with the linear amplifier, increasing the voltage up to ×80. (B) High-voltage DC field power supply. (C) The internal EF configuration reactor between plates (type 1). (D) PTFE-coated wires producing non-uniform EF (type 2, in the liquid, but non-contact, so external). External EF configuration reactors (with *d* as the thickness of the non-electrode wall): (E) circular glass bottles (type 3) and (F) a quartz cuvette (type 4). (G) Hot oil bath for immersion of synthesis reactors.

30 MHz (depending on the model used); when connected to an amplifier (with two equivalent channels), the output voltage can be increased to 800 V_{PP} (amplified 40 times, and up to 1600 V_{PP} with the combination of both channels), while the frequency is reduced to approximately 200 kHz (Fig. 2, note that this voltage–frequency dependency is non-linear, *e.g.*, at low voltages, the maximum frequency is much higher, Fig. S1). For increasing the voltage capacity even further, high-voltage DC EFs were applied *via* a separate power supply (Fug HCP14), operating at up to 20 kV with a current limited to 0.6 mA (Fig. 2B).

Initially, as the "type 1" synthesis vessels, we used 40 ml polypropylene bottles, which were manually equipped with internal stainless steel plate-like electrodes (2 cm × 4 cm, 0.125 mm thickness, RECORD), spaced 1 cm apart, to apply both AC and DC EFs up to 1600 V_{PP} (Fig. 2C). However, due to the water-splitting reaction appearing in the system (especially during high-voltage DC experiments), the setup had to be modified to eliminate the physical contact between the electrodes and synthesis solution. For this, another combination of PTFE-coated copper wires (*i.e.*, without contact with the reaction media) installed inside of 7 ml glass bottles and spaced 0.5 cm apart was explored for the application of DC EF – "type 2" (Fig. 2D). This EF configuration is essentially considered external because the electrodes are not in direct contact with the mixture. Finally, to allow for higher chances of uniform EFs throughout the entire solution volume, we utilized in-house-produced circular glass reactors and quartz-made macro cuvettes ("type 3" – Fig. 2E, and "type 4" – Fig. 2F). These setups allowed us to investigate the effects of varying solution volumes, glass wall thicknesses, and electrode spacing (which influences EF strength). The configurations enabled the application of voltages up to 20 kV in the circular reactor and up to 13 kV in the cubic cuvette.

Nevertheless, even with PTFE-coated wire electrodes, the high-voltage power supply enabled the voltage to be increased to 3 kV. Beyond this voltage, a short circuit occurred at the electrode tips due to sparking during test reactions, as shown in movie 1 (SI). To prevent the risk of glass reactor explosion, low-temperature synthesis conditions (below 100 °C) were carefully selected, with all the reactors immersed in an (electrically insulating) oil bath (Fig. 2G), while the stirring function is excluded (OHAU Guardian 5000 hot plate) in this design to minimize possible effects of magnetic fields. This interference has been observed in other crystallization systems under high-voltage EFs.[18] We also observed that spark discharges at high applied voltages (electromagnetic pulse, movie 2 in the SI) lead to the failure or temporary shutdown of the digital stirring plate. The photos and specifications of reactors are provided in Fig. S2 and Table S2.

In addition to the reactor design, selecting an appropriate synthesis system is essential for investigating the effects of EKC on crystallization. A diverse range of synthesis conditions were explored, including highly dilute and concentrated systems, IZC, CDM, and variations in the presence or absence of (in)OSDAs. Alongside, temperature is a key variable. Table S1 provides a summary of all the synthesis systems studied in relation to EKC over crystallization. The use of glass reactors introduces an additional variable due to the corrosive nature of the zeolite synthesis mixture, as it restricts the maximum alkalinity that can be employed in the system (Fig. S20).

3.3. Alternating current EF case studies

For AC EFs, immersed plate electrodes in polypropylene bottles (type 1, Fig. 2C) were used. Since we know that the potential of the water-splitting reaction is $E^{\circ} = -1.23$ V (Fig. S3), any applied voltage difference beyond that (given a certain minor overpotential) should arouse an electrochemical reaction, possibly causing changes in pH and a pressure rise (and additional local heating effects). On the other hand, AC EFs have the advantage that electrode reactions can be eliminated or minimized depending on the frequency (and thus swiftly changing bias), avoiding pH and composition changes in the solution.[59] Therefore, for the great majority of synthesis trials in this part, we have used both increased voltages and rather high frequencies.

For this investigation, we favored an EAB synthesis recipe, which is in competition with FAU. EAB also shares structural similarities with the ERI topology (also sometimes noticeable in the provided PXRD patterns at 7.8 and 13.4 2θ degrees), and where the formation of phases is simultaneous and competitive. One of the used ingredients, tetramethylammonium hydroxide (TMAOH), is famous for being a non-specific directing agent for approximately 70 zeolite frameworks. Such a system could be suitable for investigating EKC-influences on the phase direction, since we seek systems with strong rivalry between metastable phases (conditions – Table S1, entry 1).

The first attempts were run at low voltage. It is inspiring to note that only with an EF applied, the EAB-phase was noticed (Fig. S4). Nevertheless, the dependence of the frequency was slightly obscured at 10 V_{PP}. Consequently, a screening of a wide range of frequencies was introduced for an increased 20 V_{PP} bias (Fig. S5). Unfortunately, since (relatively) low-voltage was used, differences were not as conclusive as they were hoped to be. What was noticed is: (1) phase outcome has a complicated frequency dependency response – while all samples indeed show the appearance of the EAB phase (with only one outlier at 250 Hz), materials synthesized with frequencies in the range of 500 to 40 000 Hz, and 250 to 500 kHz had a higher yield of the EAB-phase, but still, its appearance is considerably small (as will be shown later), and (2) competitiveness of the silent synthesis – each of the experiment series has been carried out with a silent comparison sample, and the PXRD pattern of that sample sometimes shows a pure FAU-phase or, unfortunately, more often, a mixture of EAB and FAU-phases (Fig. S6). These findings highlight the fact of the possible non-ideality of the chosen system and the necessity of the usage of higher potentials. Non-ideality could derive from temperature or concentrations of gradients not related to EKC, starting gel preparation (while maintained as consistent as possible, still could slightly differ), poor mixing or accidental seeding.

Moreover, Fig. S7 shows two pairs of high-voltage EF syntheses at varied frequencies, which were performed to check the reproducibility of the procedure. It is essential to underline that, at first, in both pairs, PXRD patterns are not as different as it is suggested from the graph; normalization of PXRD patterns is an open question because it can depend on two factors: a diffraction intensity or the baseline. The intensity was chosen in these figures since, overall the pairs synthesized under identical conditions show very similar values. For instance, in Fig. S7, PXRD patterns of the mixed product outcome resemble each other closely, with an obvious EAB prevalence in the 20 kHz example (orange and red). However, the 5 kHz example is less straightforward; the two patterns show moderate intensity differences, with an EAB/FAU reflection ratio of 100/60 *vs.* 80/100 for blue *vs.* green, respectively (with intensities at 6.3 and 9.6 2θ for FAU and EAB, respectively, normalized to 100). This does indicate some variability in the relative phase proportions between the two runs. Yet, regardless of the quantitative variation, the clear presence of the EAB phase in both patterns suggests a prominent EKC effect. In the following trials with a high voltage (*i.e.*, 1000 V_{PP}), the yield of the EAB phase was much higher than before, and the pure EAB zeolite was formed for the low-frequency sample (500 Hz). It is remarkable for these syntheses that both parameters (*i.e.*, V_{PP} and Hz) seemed to play an essential role in the formation of the appropriate zeolite phase.

With the desire of bringing these trials even further, a wide screening of voltage/frequency (0–800 V_{PP}; 50 μHz–30 MHz) combinations was conducted in sealed polypropylene bottles with immersed stainless steel electrodes (type 1). Since the amplifier had two channels, only two parallel voltage-assisted reactions were executed along with comparative silent samples. Eventually, in order to have a set of 4 tests managed by voltage control (*i.e.*, 200, 400 and 600, 800 V_{PP}), 2 series of experiments were operated, producing 2 outcomes for a blank sample, lowering a possible error of the reference (Fig. S8–S14, dashed and solid lines for "NoE"). Lastly, here and further, it is crucial to emphasize that the delivered voltage value by the amplifier could differ drastically *versus* the set one due to its frequency response (see Fig. S1); therefore, the conclusion should be drawn more carefully if the frequency value exceeds 100 kHz.

Unfortunately, several tests at the micro-hertz frequency, *i.e.*, 50 μHz (all along the 72 hours of synthesis, polarity changes every ~2.8 hours), resulted in overdried gels, probably due to excessive evaporation along with the water-splitting reaction. Therefore, in order to achieve more reliable results, the lowest tested frequency in further experiments was set at 50 mHz. In another low-frequency trial, we attempted to cover some theoretical approximations, seeking the best EF-driven influence on the bulk synthesis. Accordingly, the "characteristic frequency" of the parent solution was estimated to be around 787.6 Hz (see the Methods section), and was used in the screening. Nevertheless, the used frequency did not showcase a vital effect on the zeolite crystallization, since all samples (Fig. S8) possess a mixture of both phases (as do a great majority of the blank runs) with very similar Si/Al ratios around 3.4. The high-voltage experiment was repeated twice, resulting in two diametrically opposite patterns, which suggests that the observed effects are not consistent.

Furthermore, the frequencies were increased even more, and these tests suggest that all of the EF-made samples did exhibit a similar pattern with the EAB phase prevailing and Si/Al ratios lowered towards 3.0. While the best selectivity was reached for 50 (Fig. S11) and 100 kHz (Fig. S12) high-voltage experiments, tests at 30 MHz frequency (Fig. S14) behaved rather unusually with much lower crystallinity and increased formation of FAU.

Finally, Fig. 3 presents the whole list of scanned frequencies for 800 V_{PP} voltage. A complex motif can be noticed with two EAB phase-selective regions: at low- (0.05–787.6 Hz) and high-magnitude (0.04–1 MHz) frequencies. We tend to attribute the outcome synthesized at the highest frequency – 30 MHz – to a generator error/threshold of the amplifier capability (the ability to scale up a signal is frequency-dependent, *i.e.*, the voltage has a limit at higher frequencies, Fig. S1). Therefore, we anticipate that there is a middle range in the frequency

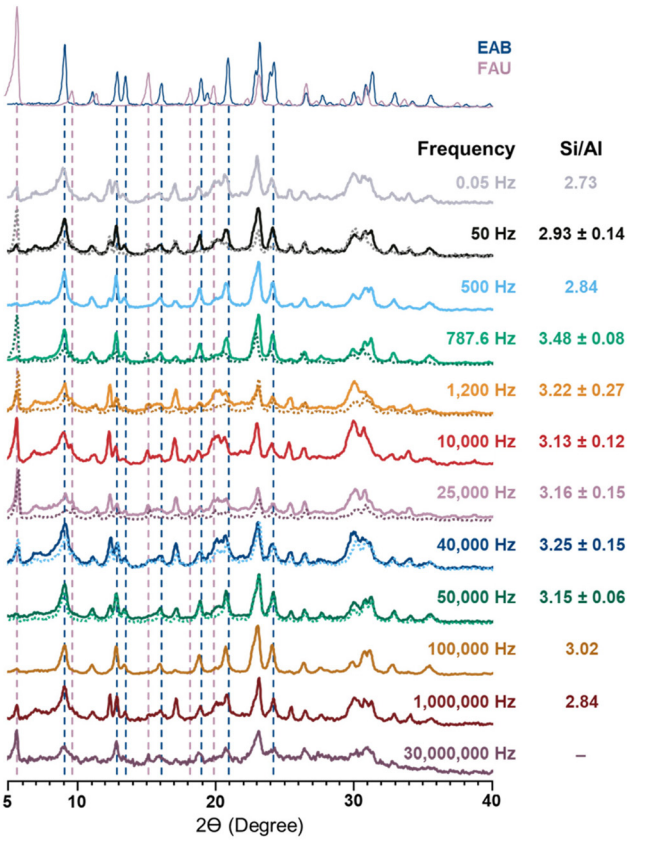

Fig. 3 The overview of the wide-range frequency influence screening for the competitive EAB/FAU transformation system at the fixed 800 V_{PP} voltage. EAB and FAU model diffractogram simulations are found on the top; the most intense reflections are referenced with dashed lines of a corresponding color. For 50; 787.6; 1200; 10 000; 25 000; 40 000 and 50 000 Hz, two repetitions of the syntheses were conducted; the results were analyzed by ICP separately.

values, which does not assist in conditions to selectively yield the EAB phase. The estimation of the calculated characteristic frequency, which is designed to shake the system out of existing equilibria, has been (to a certain extent and with doubt) correct since the (almost) pure-phase EAB zeolites were synthesized in these frequency zones – a result opposite to the majority of the silent system results yielding FAU.

ICP analysis was performed for most of the EAB/FAU samples (right column). Results for that series were rather inconclusive, and thus we have only a theoretical suggestion: in case of a mixture of two zeolites, their precise phase composition (wt% EAB *vs.* total, *e.g.*) could not be easily established. However, as the EAB zeolite generally has a slightly higher Si/Al ratio, mixtures with the dominant EAB phase are supposed to be (a bit) more silicon-rich. This way, some of the samples with the more dominant EAB phase as seen in PXRD measurements were indeed found to have higher Si/Al ratios.

Finding EKC by AC EF in bulk zeolite synthesis could also bring a sparkle of hope for a better understanding of zeolite crystallization during the nucleation stage.[14,16] Unfortunately, the scientific literature on the nucleation step or on the initiating stages of crystal growth processes for even the most common zeolites is very scarce.[60] Difficulties in zeolite framework formation studies arise from the often highly inhomogeneous nature of the gel or synthesis mixture multiplied by the countless number of independent parameters one can vary. New insights into the very early stage events of zeolite crystallization are highly desired.[61]

As some of the phase-selective experiments were conducted in the competitive EAB/FAU system, we expected that some of the changes in phase selectivity originate from an EKC-influenced nucleation stage. While the approach of having an investigation on nucleation of simultaneously growing zeolite phases is arguable from a classical point of view, we underline the great importance of nucleation as a crystallization event by demonstrating its ability to direct a synthesis outcome (in terms of phase produced). For exploring that point, a modified series of experiments were performed with partial EF assistance, in contrast to the above EF-assisted experiments, where the procedure was run for three uninterrupted days with voltages on (or off for silent samples). The first stage of this investigation consisted of five samples: a blank sample without electricity, while the four residual samples have had 400 V_{PP} at 50 kHz: during the first 24 hours (from the total of 72 hours), the second 24 hours, the third 24 hours, and the entire 72 hours of the experiment (see the legend on the right of each diffractogram in Fig. 4A). In this way, the first 24 h period should be essential for the nucleation stage, *e.g.*, for both '1st 24 h 400 V_{PP}' and 'full 72 h 400 V_{PP}' experiments.

For samples that were conducted with EF on during the first 24 hours, the formation of the FAU zeolite was overruled by a pure EAB phase. For the others, the formation of the FAU phase was still noticeable. Given a classic S-curve in crystallization and the short time of these syntheses, the nucleation phase likely falls in day 1. The distinction in the results of silent control syntheses from all others conducted with electricity is remarkable, and this could mean that with the applied high-voltage EF, we are indeed changing the nucleation kinetics.

A series of additional experiments were done for forming a more complete understanding of the EAB/FAU mixture nucleation under an applied internal EF. This time, higher voltages and different times and frequencies were used: 800 V_{PP} with 50 kHz or 50 mHz was applied for 6, 24, or 48 hours from the beginning of the 72-hour experiment (Fig. 4B and C). It needs to be mentioned that for every paired experiment in the series, each mother solution was prepared (always with the same procedure), which is why we may have an artifact (an outlier) for the 48-hour electric synthesis, as it gives a higher than expected yield of the FAU phase. For the others, in both cases, the most intense reflections of FAU are found for the synthesis without electricity. Nevertheless, when applying the EF, the selectivity towards EAB rises. Notably, the pure phase EAB was synthesized in the 6-hour experiment (1st 6 h 800 V_{PP}), and the yield of EAB decreased with the prolongation of applied electricity time. This finding indicates that constantly applied EFs could cause divergent effects on bulk zeolite synthesis, which could overtake each other, adding an extra level of complexity, as has been seen in the previous experiments. In addition, SEM analysis of 6- and 72-hour samples (800 V_{PP} with 50 mHz) was performed (Fig. 4D), and smaller crystals were found for a shorter time of influence, suggesting a superior amount of initial crystallization sites (and thus impacted nucleation). Therefore, the rearrangement and pre-nucleation ordering, which happens in the first few hours of the experiment, is likely the most significant for the future phase selectivity and the most likely to feel EKC influences. In the end, comparing these experiments by their difference in the frequencies of the EF (Fig. 3), we suggest that, for the high-frequency system, the formation of the FAU phase was rather more suppressed.

In conclusion, the influence of a strong EF on bulk zeolite crystallization was found to have a more pronounced effect on the phase selectivity in the competitive system of EAB/FAU (*vs.* low voltages), but still seemingly hard to understand (or reproduce). Nevertheless, these results, especially the manipulation of nucleation kinetics, seem to be the first demonstration that it is possible to control the phase-selectivity of zeolite synthesis with a high-voltage EF and that the impact of EKC is most likely found in the first stages of crystallization. It opens prospects for many exciting directions for future investigations since such effects have never been described.

3.4. Direct current EF case studies

EKC investigations were continued with the competitive EAB/FAU syntheses. Here, syntheses were conducted in 7 mL glass vials equipped with PTFE-coated electrodes inserted in the liquor (type 2, Fig. 2D). The results and discussion for these experiments are provided in the SI. Subsequent trials with the type 2 reactor focused on the synthesis of FAU/LTA, where the phase selectivity shifted from FAU to LTA upon replacing NaOH with TMAOH,[51] using the gel molar composition

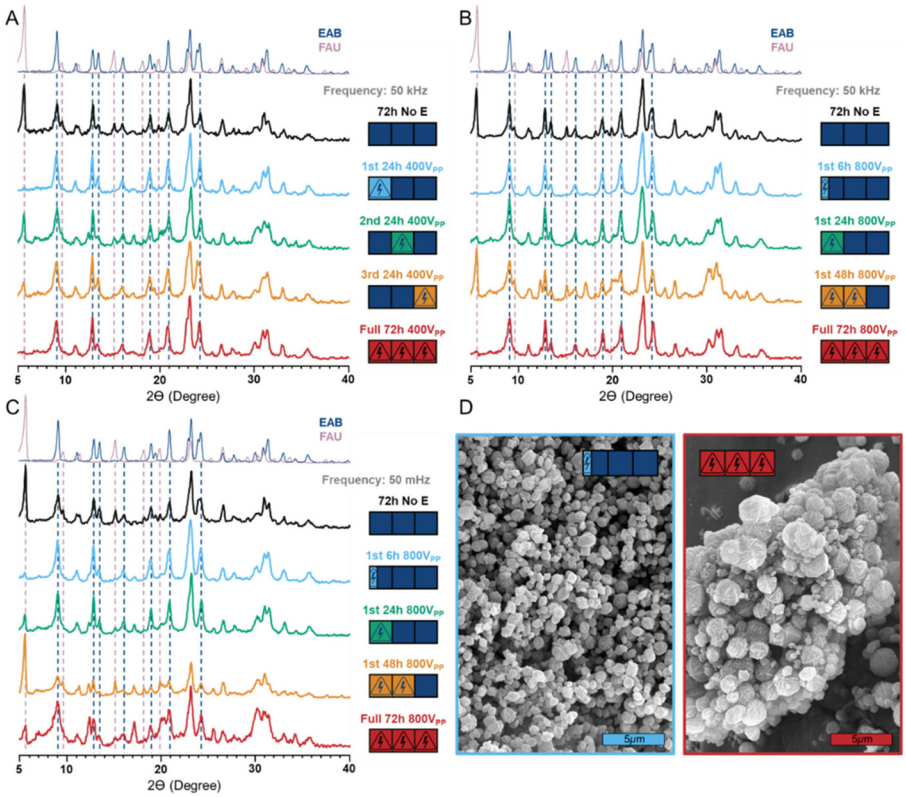

Fig. 4 PXRD patterns of the nucleation study: (A) three separately tested different days of applying internal EF of 400 V_{PP}, 50 kHz frequency with silent (0 h, darkest, no E) and full 3 days (72 h, red) of EF references. Internal EF of 800 V_{PP} with (B) 50 kHz and (C) 50 mHz frequency applied in the initial stage of the synthesis for 624 and 48 h with silent (0 h, darkest) and full 3 days (72 h, red) of EF references. (D) SEM pictures of the zeolite synthesized in (C) 6 (left) and 72 (right) hours of EF; both pictures were captured under the following conditions: SEI mode, 15 kV accelerating voltage, working distance of 10 mm, spot size 40, ×5000 magnification; the scale bar corresponds to 5 μm.

described in Table S1, entry 2. In the absence of NaOH, no solid product was witnessed even after 7 days at 100 °C. However, when an EF of 800 V_{PP} was applied for 4 days, an amorphous solid with traces of crystallinity was obtained (Fig. S17A). The observed reflections were difficult to assign to a known framework, and the experiment was not reproducible, even at higher EFs up to 20 kV. By increasing the NaOH/Si molar ratio to 0.012, FAU was successfully formed under all three conditions: batch synthesis, 0 V, and with an EF of 400 V_{PP} (Fig. S17A); however, the yield under EKC was about 75% lower. When the NaOH/Si ratio exceeds 0.012, LTA begins to co-crystallize alongside FAU, eventually becoming the dominant phase at a 0.06 ratio in both batch and 0 V syntheses. Interestingly, under an applied EF of 400 V_{PP}, the phase selectivity shifts toward LTA at significantly lower NaOH/Si ratios. In this case, LTA becomes the dominant phase already at a NaOH/Si ratio of 0.024 and forms a pure-phase LTA at a ratio of 0.04 (Fig. 5A). The intensity ratio of the characteristic PXRD reflections for FAU (2θ = 5.9) and LTA (2θ = 7) clearly illustrates this shift in phase selectivity toward LTA under the influence of the EF, compared to batch and 0 V conditions (Fig. 5B). Complete PXRD patterns for all samples are provided in Fig. S17.

As the NaOH/Si molar ratio increases from 0.016 to 0.04, the Si/Al ratio in the resulting materials decreases, coinciding with a phase selectivity change from FAU to LTA.[62] This decline in Si/Al ratio becomes more pronounced under an applied EF, deviating further from the trends observed in batch and 0 V_{PP} syntheses (Fig. 5C). The formation of LTA is favored at higher NaOH concentrations, where the increased availability of sodium facilitates aluminum incorporation into the framework. This observation led to our hypothesis that the local concentration of Na^+ can be modulated by an applied EF, thereby influencing the kinetics of crystallization. Furthermore, due to the transparency of the silicon oil and glass vials, the progression of crystallization could be qualitatively monitored through changes in the turbidity of the reaction mixtures. Crystallization was initiated from a clear solution, with the onset of turbidity serving as a visual indicator of nucleation. Fig. S18 and S19 present time-resolved images of the synthesis vials for NaOH/Si ratios of 0.024 and 0.04, respectively. Under the applied 400 V_{PP} EF, the crystallization was initiated more rapidly. After 42 hours, the solid obtained from the synthesis with a NaOH/Si ratio of 0.024 under EF was pure LTA. Extending the reaction to 72 hours led to the emergence of FAU as a minor phase. In contrast, at a NaOH/Si ratio of 0.04, the product remained pure LTA even after 72 hours under EF, suggesting that FAU formation is either significantly delayed or entirely suppressed by the EF.

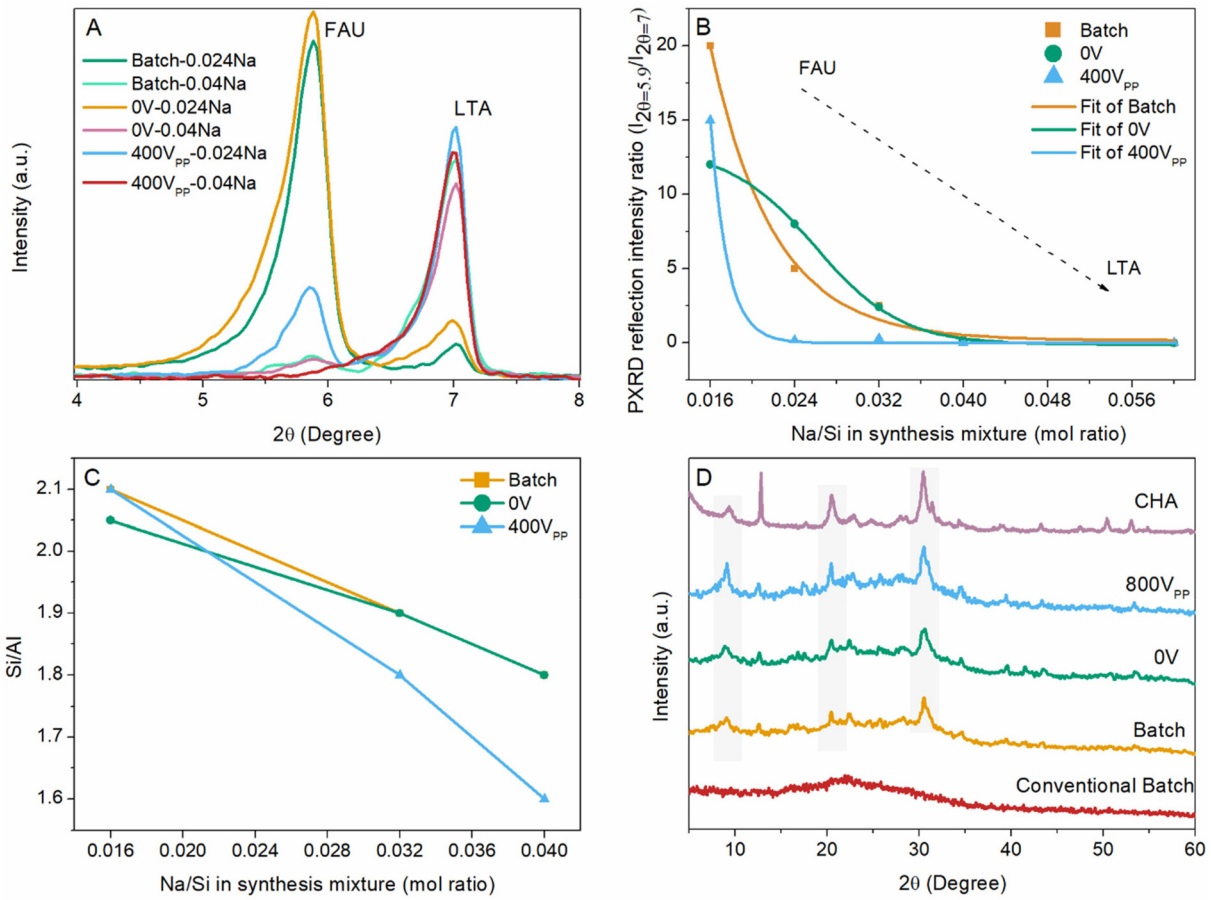

Fig. 5 (A) PXRD patterns of the samples derived from FAU/LTA synthesis at 100 °C, with NaOH/Si ratios of 0.024 and 0.04 after 72 h. (B) Intensity ratio of PXRD characteristic reflections of FAU and LTA *versus* the amount of NaOH in the synthetic gel (Na/Si). (C) Si/Al ratio of FAU/LTA samples *versus* the amount of NaOH (Na/Si) and (D) PXRD patterns of samples derived from CHA syntheses after 96 h at 100 °C. The PXRD pattern of nano-sized CHA is taken from the IZA database. A batch means the same vial used for EKC and 0 V but without electrodes (0 V has electrodes inserted), while a 'conventional batch' means a Teflon-lined stainless steel autoclave.

To further explore the hypothesis (*i.e.*, link between the inorganic cation (Na^+) and EF and the concomitant favoring of LTA), another EKC synthesis (in the type 2 reactor) was performed using a system that necessitates an (in)OSDA cation with higher valence. In this context, the crystallization of the low-silica CHA zeolite was investigated with the strontium cation (Sr^{2+}), serving both as an (in)OSDA and as a crystallization accelerator.[50] With a Sr/Si molar ratio of 0.01 (Table S1, entry 3), after heating for 72 h at 100 °C, the crystallinity of the product under 800 V_{PP} is mildly higher compared to batch and 0 V (Fig. 5D). This improvement in crystallinity might appear due to the EF affecting the local concentration of Sr^{2+} in the bulk. In the original study, the Sr/Si ratio of 0.01 was identified as the optimal concentration for complete crystallization of CHA after 24 h. Variations in synthesis time in our case could be due to differences in reactor configurations; however, similar synthesis in a conventional batch (Teflon-lined stainless steel autoclave) resulted in an amorphous phase (Fig. 5D). More to that, using glass vials for CHA synthesis surprisingly led to wall corrosion due to the system's extreme alkalinity, introducing sites for heterogeneous nucleation and compromising the comparison (Fig. S20A). In contrast, polypropylene vials (type 1 but with PTFE-coated Cu-wire electrodes) suffered from leakage issues caused by material softening at high temperatures (Fig. S20B), rendering the results inconclusive.

The preliminary results for the FAU/LTA system lead us to propose a mechanism for phase formation and selectivity under EKC conditions. Na^+, having a higher charge density than tetramethylammonium cations (TMA^+), can migrate more readily toward the negative electrode under a direct current EF, creating a local supersaturation that favors the formation of double four rings (d4r, a cube, see Fig. 6A) – the characteristic composite building units of the LTA framework. The formation of d4r and sodalite cages, only the latter are shared between both FAU and LTA topologies, likely shifts the phase selectivity toward LTA at the same sodium concentration, whereas batch conditions typically favor FAU (Fig. 6A). Additionally, higher sodium concentrations promote aluminum incorporation into d4r units, resulting in a higher aluminum content in the LTA phase (Fig. 5C). It has been observed that FAU crystallizes

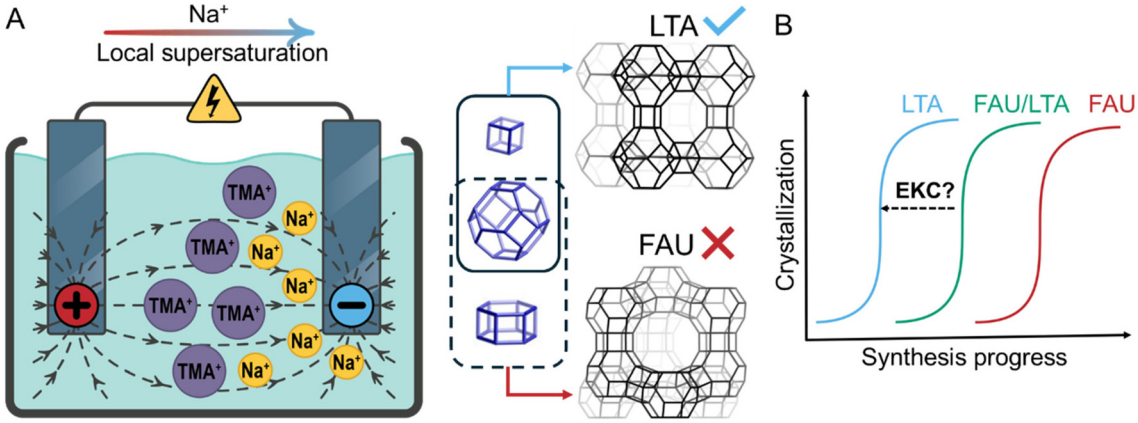

Fig. 6 (A) Hypothetical mechanism of LTA selectivity under EKC and (B) kinetics enhancement of LTA and FAU phase separation under EKC. TMA^+ = tetramethyl ammonium cations.

more slowly than LTA, with mixed FAU/LTA phases exhibiting intermediate kinetics.[63] EKC facilitates the separation of LTA and FAU phases and enhances the crystallization kinetics of LTA (Fig. 6B). This mechanism is considered reliable and rational, as a similar behavior has been observed in solid separation from mixed suspensions.[18] However, the reproducibility of the experiments was again slightly problematic, particularly in the presence of internal electrodes, adding extra heterogeneity. The inconsistent results of the synthesis of FAU/LTA and trials for FAU/LTA without OSDA,[45] FAU/EMT,[43] nano-sized NaA zeolite,[49] Na-UZM-9 [48] (LTA framework) and BPH[47] systems using the type 2 reactors are provided in the SI.

To apply higher voltages and incorporate non-contact electrodes with media, aiming to minimize potential interference and enhance the field control, we utilized custom-made circular glass bottles and a quartz cuvette (Fig. 2E and F, types 3 and 4). Initially, we replicated the FAU/LTA synthesis at 800 V_{PP} using a 30 ml circular bottle (type 3), where LTA was still the dominant phase at a NaOH/Si ratio of 0.032, being consistent with previous results. However, when higher voltages were applied, *e.g.*, 12 kV and 20 kV with type 3, 30 and 8 ml circular bottles (Fig. 2E), and 10 kV with the type 4 reactor (Fig. 2F), the system favored FAU formation already at a NaOH/Si ratio of 0.024, contrary to our initial findings (Fig. 7A and B). In the latter experiment (10 kV, type 4), the Si/Al ratio was also similar to that observed under batch conditions (Table S4). Interestingly enough, the kinetics of this system, along with the heterogeneous nucleation, are strongly influenced by the shape of the reactors. This results in significant variations in crystallization, which are extremely time-dependent on the reactor geometry.

In the effort to elaborate on the interplay between reactor geometry and EFs on nucleation and selectivity of a synthesis, we also tried two more systems: nano-sized silicalite-1 (MFI, Fig. 7C) and an embryonic CHA (short-range order CHA crystals, Fig. 7D), limiting ourselves to the quartz cuvette settings (type 4). Nevertheless, the PXRD patterns of materials crystallized under batch and EKC conditions were identical as well as their particle sizes (Fig. S25). The Si/Al ratio was also similar for EKC and batch conditions in the embryonic CHA zeolite (Table S4). The proximity of framework Al was also assessed through divalent cation capacity (Co^{2+} exchange). Both CHA samples, synthesized in batch and under EKC, exhibited a similar Co/Al ratio of 0.23, indicating that EF shielding does not influence the Al sitting strongly within the lattice under these conditions.

Next to unclear effects of the EF on phase selectivity and particle size, its impact on the solid yield was mixed and dependent on the specific zeolite system. For FAU/LTA under a non-uniform EF (7 ml vials, type 2, Fig. 2D), the yield for EKC was generally lower than those under batch and 0 V conditions. Similarly, under uniform EF (type 4), the EKC sample showed a reduced yield. In contrast, for MFI, there was no observable difference in yield between EKC and batch conditions. However, in embryonic CHA, EKC resulted in a higher yield compared to batch synthesis.

3.5. Discussion

Based on our mixed results showcased for both AC and DC EFs in EKC during zeolite crystallization, together with the nature of zeolite synthesis and the existing literature on EKC in crystallization, we can wrap up with a discussion. The first thing to consider is the extent of dipole energies under an EF (the energy of a dipole due to orientation under an EF). Dipole energies remain small compared to thermal energies, as $\mu E \ll k_B T$ (μ is the dipole moment, E is the electric field, k_B is the Boltzmann constant and T is the absolute temperature). However, EFs in the range of 40–200 kV cm^{-1} have been shown to influence the net molecular orientation and thermodynamic potentials for proteins.[64] Zeolite synthesis media are typically highly ionic due to the presence of various dissolved ions, and when a DC EF is applied across such a medium, electrical double layers (EDLs) form at the surfaces of the electrodes or the charged surface.[65] These EDLs shield the applied field over a characteristic distance known as the Debye length (Fig. 8A, DC).[65,66] Within the EDL, mobile ions rearrange to counterba-

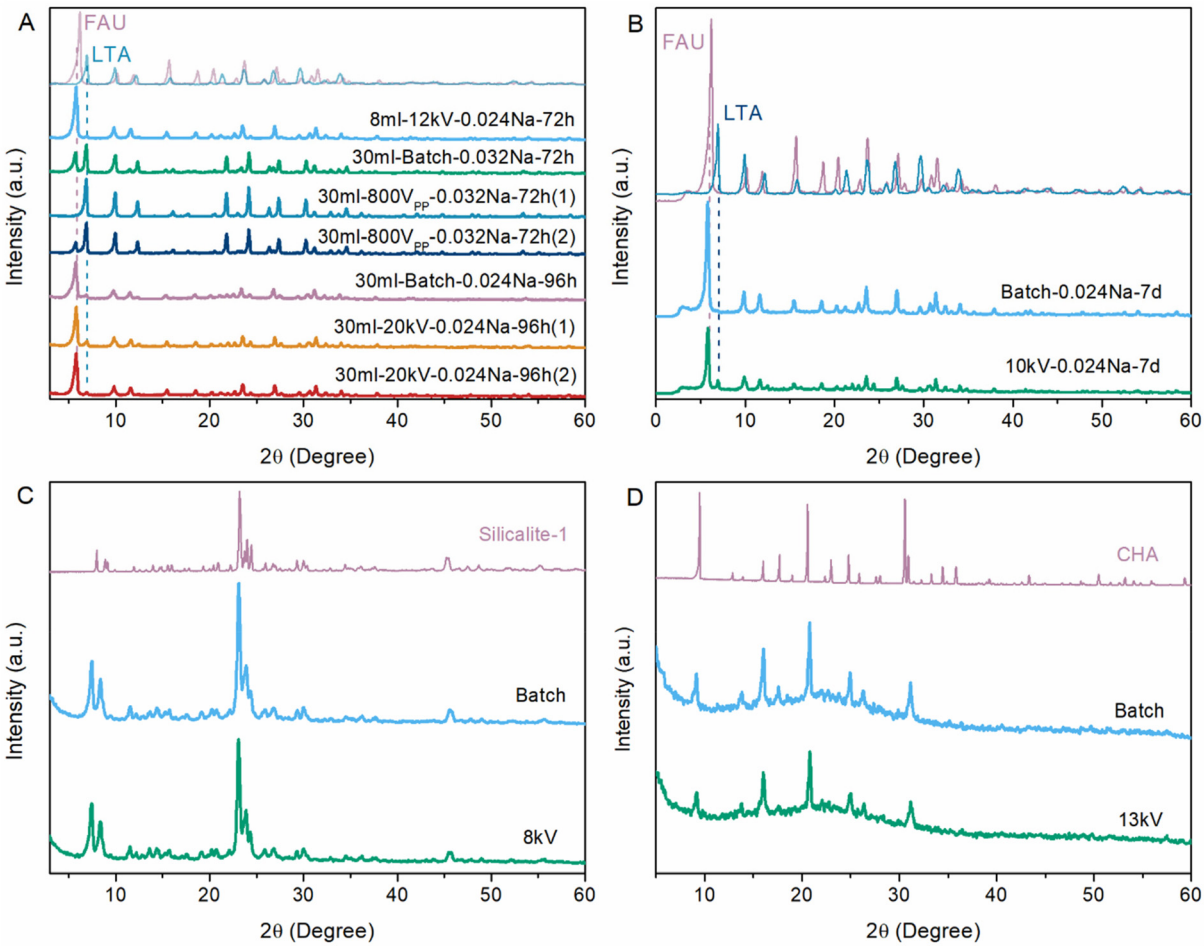

Fig. 7 PXRD patterns of products obtained from the synthesis of the FAU/LTA system in (A) circular bottles (type 3), (B) a quartz cuvette (type 4) and (C) MFI, and (D) embryonic CHA zeolites in a quartz cuvette (type 4). FAU and LTA reference patterns were measured from CBV300 (zeolyst) and zeolite 4A. Silicalite-1 and CHA reference patterns were collected from the IZA database. The photos of the syntheses in quartz cuvettes are shown in Fig. S24.

lance the external charges induced by the field (Fig. 8B). As a result, the EDLs effectively act as insulating layers, preventing the EF from penetrating deeply into a bulk solution. Therefore, the EF in the bulk solution is likely practically zero.[65] For instance, considering the synthesis mixture for FAU/LTA (Na^+/Si = 0.024, TMA^+/Si = 1.096 and OH^-/Si = 1.12) the theoretical Debye length (Debye–Hückel) is 2.62 nm in the case of Na^+. The applied EF is then only effective at these lengths, where it decays exponentially within this length according to the Poisson–Boltzmann equation.[15] Also, the voltage drop in the quartz wall (type 4 or in the Teflon coating of wire electrodes, type 2) is linear and inversely proportional to the dielectric constant of the quartz (or Teflon, Fig. 8A). In contrast, the assumptions of the EDL theory can be less applicable at high ion concentrations (≥0.01 mol L^{-1}) and voltages (≥52 mV for the surface potential).[67] In our case, the concentration of ions is significantly higher (for only OH^-, it is 1.11 mol L^{-1} H_2O), which can still compensate for the charges induced by an EF of even 20 kV through packed multilayer counterions[68] (by considering ideal capacitance behavior). At high potential and electrolyte concentration, the Poisson–Boltzmann/Gouy–Chapman theory underestimates the screening length of the potential.[68–70] Under these conditions, the Debye length can increase due to strong interactions of ions (even 100 times thicker).[70] Although the Debye length increases (yet remains within the nanometer range), the high ion concentration causes the EF sensed in the bulk to decrease. The EF decay has been measured in bipolar electrodeposition, where within 1–2 minutes, the EF in the bulk drops to below 30% of the applied potential.[71] We also attempted to measure the voltage inside the solution using the linear amplifier and the circuit shown in Fig. S26. However, due to significant voltage fluctuations, obtaining an exact measurement was challenging *via* a simple multimeter. Nevertheless, when a set voltage of 800 V_{PP} was applied, the thin wire probe in contact with the inner wall of the cuvette (type 4) sensed the real voltage to change from 15 to 100 V, which gradually dropped to 0 V after a few (≤1–2) minutes. The formation of the EDL is on the order of pico- to microseconds, but the EF decay on the order of minutes can be due to macroscopic ion migration (accumulation on both

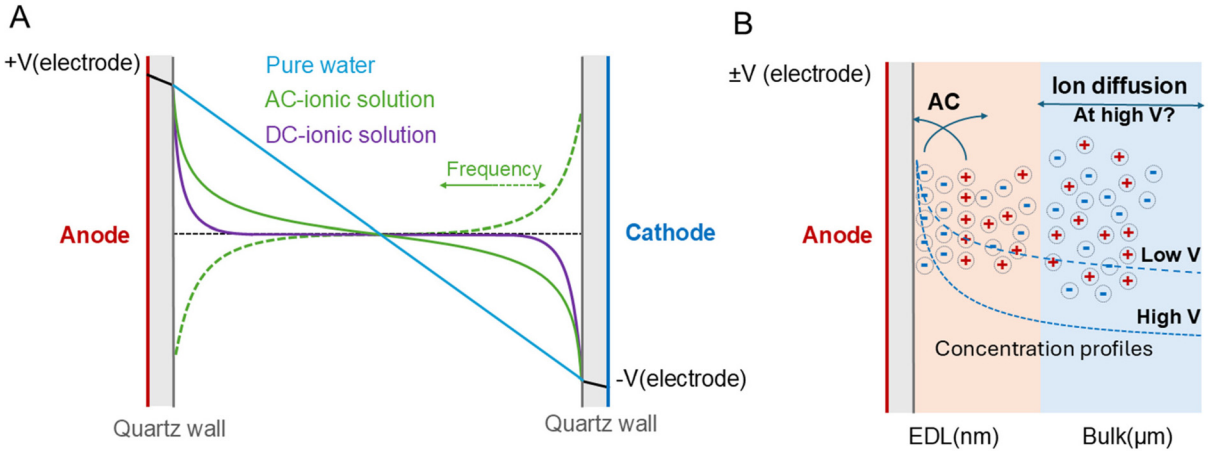

Fig. 8 (A) Hypothetical voltage profiles through a quartz cuvette (type 4) including synthesis solutions under AC (frequency represents high enough frequencies with time ranges shorter than EDL formation, MHz–GHz) and DC EFs. The profile inside pure water is added for comparison with the cases where ions are present in the zeolite synthesis solution. (B) Qualitative ion migrations and concentrations through the electrical double layer (EDL) and micrometric scale diffusion layer close to the EDL.

sides).[71] The concentration profile of ions in the solution depends on the applied EF properties. Under low DC EF conditions, the concentration of counter ions increases steeply within the EDL, and a diffusion (Nernst) layer develops whose thickness depends on time and the diffusion coefficients of the species (Fig. 8B, concentration gradient in low V). At high DC EF amplitudes and high ionic concentrations, ion migration close to the electrode can involve multilayer counter-ion accumulation, and diffusion from and toward the bulk can differ. The enhanced diffusion triggered under such conditions (Fig. 8B, concentration gradient in high V) may introduce time scales on the order of seconds to minutes for EF effects to be sensed in the bulk. These observations, along with the theoretical considerations of electrode polarization and the EDL, suggest that the effective EF is confined to a very narrow region near the inner wall and does not penetrate into the bulk of the solution (or only shortly). Nevertheless, sensing fine voltages on the order of millivolts across nanometric-scale regions has proven to be effective in manipulating protein crystallization.[4] The relevance of such phenomena to zeolite synthesis, however, remains ambiguous. Using AC EF can prevent the formation of the EDL by changing the polarity below the decay time range (Fig. 8A, AC). In the AC mode, periodic reversal of EDL charging hinders the formation of a sustained concentration gradient extending from the EDL into the bulk (Fig. 8B). The effects of high-voltage EFs on the thermodynamics of protein nucleation depend on the change in dielectric constant between the solid and liquid phases.[4] The variation in dielectric constant with component composition determines the change in chemical potential during the phase transition (nucleation). In the case of protein, the effects are mainly confined to size and quality of crystals, nucleation rate and number of crystals. In the case of zeolites, investigating changes in the dielectric constant of the solid phase may be nontrivial due to the similar electrical properties between intermediate amorphous phases and final crystalline structures, not to mention the potentially changing dielectric constant of the liquid/gel. However hard to predict the changes in chemical potential under the EF, particularly those derived from frequency shifts, an EF could lead to the formation of a different zeolite than that expected in conventional synthesis, since the thermodynamic states of the initial gels (preordered stages including oligomers and building units) for various frameworks do not differ significantly (so an EF-induced change could be significant).

4. Conclusion and outlook

In this study, we report for the first time attempts to use high-voltage electric fields (EFs) to control bulk zeolite crystallization. The inability of classical kinetic laws to govern hydrothermal synthesis sufficiently led us to hypothesize that these limitations arise from complex interactions spanning the transition from pre-ordered to ordered stages of zeolite formation. Since the synthesis mixture contains various ions, and the crystallization of aluminosilicates introduces charge defects that require electrostatic stabilization, electrokinetic control (EKC) presents an intriguing approach to manipulate both the thermodynamics and kinetics of the crystallization process. Nucleation thermodynamics can be modified under high-voltage EFs, which in turn may influence the kinetics of nucleation, growth and crystallization as well as defect stabilization. The movement of charged species can also influence the temporal dynamics of reactive intermediates and local concentration gradients, which can also possibly alter the phase selectivity and the kinetics of crystallization, and potentially influence the aluminum content in the final structure. Both AC and DC EFs were investigated, with voltages and frequencies as high as 20 kV and 30 MHz. In addition, various reactor

configurations were explored to address the challenges of applying EFs during hydrothermal synthesis. The different setups enabled us to investigate both uniform and non-uniform EF modes. However, the use of Teflon-lined stainless steel autoclaves posed limitations, prompting a shift to plastic- and glass-based reactors. While glass offers compatibility with EF applications, it also restricts the synthesis conditions, particularly in terms of temperature and alkalinity. We examined the influence and effects that arose from EKC across ten different zeolite synthesis systems, each with varying compositions, conditions and viscosities. The effects of EFs on nucleation thermodynamics were evaluated in terms of phase selectivity, particle size, and yield.

Initially, our investigation of directing phase selectivity in the competitive system of EAB/FAU provided a complex output, for which further experimentation would be needed to support the hypotheses and find an explanation for the issue of reproducibility. The least inconclusive results were obtained applying EFs of 800 V_{PP} with 50 mHz and 50 kHz frequencies during the initial stages of the synthesis, more precisely in the first 6 h (although an EF during the first 24 h at 400 V_{PP}, 50 kHz also shows promise), where we observed a strong preferential phase shift *vs.* the silent controls, but, even more importantly, we witnessed an increase in the number of nuclei *via* a (roughly) 3-fold decrease in crystal size. This points to a real chance that EF can tune or influence nucleation at the very start of a crystallization and could thus be effective up front. Yet, applying EF all along the duration of a synthesis might promote other effects (*e.g.*, in the growth stage, local heat dissipation effects) at later times, which then obscure or mitigate the earlier effects on nucleation. We surmise that such later-stage EF effects could be a source of reproducibility issues. Based on our extensive preliminary data, higher voltages and a more broad frequency range should be tested. A rationale for the latter is a previous report that external EFs could relax the hydrated ion structure at significantly larger time scales (between 300 ps corresponding to 1 THz or higher) compared to most other relaxation processes in solutions;[72] therefore, tests with these extreme frequency values, if achievable instrumentation-wise, could be beneficial. Also, there are countless available combinations of starting ingredients that could yield more promising results (*e.g.*, IZC or dual-template syntheses). On the other hand, the demonstrated phenomenon of EKC over microporous material crystallization underlines the crucial role of nucleation in zeolite synthesis among competing phases and establishes the first proof of controlled phase selectivity under applied internal EF in the bulk. Moreover, we observed that non-contact EKC under non-uniform EFs could sometimes alter the selectivity in FAU/LTA systems depending on Na/Si ratios. We hypothesize that the local concentration of sodium close to the electrodes is influential. However, challenges in reproducibility emerged (again), and the application of high-voltage EFs yielded mixed results across different experiments. In this example, in particular, we surmise that heterogeneous nucleation (*e.g.*, seeding from remaining debris of a previous synthesis in the Teflon electrode sleeve) affects the outcomes of crystallization, raising doubts about the acquired EF results. Based on this, we suggest selecting systems for further studies that are inherently more prone to homogeneous nucleation (nevertheless, external nucleation modifiers could be considered in other lines of research). Case studies involving other zeolite systems also did not reveal a clear influence of EKC. The properties of the EDL formed in the highly ionic zeolite synthesis mixture are suspected to play a critical role in determining the effectiveness of EFs in the bulk. The formation of a densely packed, narrow EDL can prevent the EF from penetrating into the bulk solution, thereby reducing its influence on the crystallization process. In dilute, single-component protein systems, even millivolt-scale potential differences can influence the thermodynamics and kinetics of nucleation and crystallization through their effect on nanoscale EDLs. In contrast, zeolite systems typically contain excess concentrations of components, particularly SDAs and OH^-, which often makes local nucleation and crystallization more dependent on bulk properties. In this context, the local film deposition of zeolite on the electrode *via in situ* nucleation and growth suggests that the film shares similar properties with zeolite crystals formed in the bulk under identical conditions, with the possible exception of crystal growth orientation. Furthermore, opposite to proteins, nucleation is not always the rate-limiting step in zeolite synthesis, as the process involves multiple stages with different rate-determining steps depending on the system. Additionally, electrostatic interactions among charged species do not appear to be the limiting factor in zeolite synthesis, particularly in systems with excess concentrations of charged SDAs, OH^-, and sometimes aluminum. The contribution of steric stabilization, hydration and van der Waals interactions can outweigh the electrostatic stabilization. However, in rare cases, such as high-aluminum or dilute CDM systems, coulombic stabilization can play a critical role in driving nucleation,[48,56] where under an EF, there were no clear effects on a CDM system as well.

When the EF would consistently be able to penetrate the bulk, the greatest likelihood of effects arises from charge- and particle-based movements under this EF, as seen in electrophoretic film deposition. Under an EF, the Coulomb, electrophoretic, dielectrophoretic, and chaining forces are dominant. Dielectrophoresis requires a strong EF gradient, which restricts its influence to non-uniform fields. The chaining force has also been used for packing zeolite particles, but typically under AC EFs and specific setup configurations. In the highly ionic zeolite synthesis mixture during crystallization, electrophoretic forces are likely to dominate. Nevertheless, thermal motion at the elevated temperatures of zeolite syntheses can counteract or even override these effects, perhaps locally, intermittently, or nonuniformly. This is a likely origin of irreproducibility.

Future trials of EKC in zeolite crystallization could benefit from small-scale reactors, such as nano/microchannels or microdroplets, to limit the number of crystals formed and enhance the influence of EFs. However, this approach may require *in situ* characterization techniques, such as XRD, to

monitor crystallization timely and effectively. Another promising strategy involves applying high-voltage AC EFs with a broader frequency range (high frequencies in the MHz–GHz range), particularly in setups using external plate electrodes. Using water as a solvent (cfr., with its high dielectric constant and conductivity in ionic solutions, both of which vary significantly with temperature) can be a drawback for studying EKC in zeolite crystallization. Less polar solvents or ionic liquids may offer better compatibility with EF application; however, crystallization systems using these alternatives are still scarce.[2] Theoretical and mechanistic studies on the effects of EF on temporal changes in dielectric permittivity of emerging solids, as well as on interactions of atoms within the lattice and with extra-framework cations, can be useful for a clearer understanding of EKC over zeolite crystallization.

Author contributions

M. T. B.: writing the original draft and the DC EF part and its experiments. G. I.: writing the AC EF part and its experiments, reviewing, and revising. M. D.: funding, reviewing, writing, editing, and supervising. All authors have conceived and reflected on the concepts in this work.

Conflicts of interest

The authors declare no competing financial interests.

Data availability

The data supporting this article have been included as part of the supplementary information (SI). See DOI: https://doi.org/10.1039/d6dt01004k.

Acknowledgements

M. T. B., G. I., and M. D. thank the European Research Council (ERC) for funding: ERC Starting Grant 948449 named Z-EURECA, *i.e.*, ZEolite synthesis in Unusual Reactors for Enhanced Catalysts to MD.

References

1 C. Baerlocher and L. B. McCusker, Database of Zeolite Structures. Available at: https://www.iza-structure.org/databases/, 2014, accessed online: June 2019.
2 A. Deneyer, Q. Ke, J. Devos and M. Dusselier, Zeolite Synthesis under Nonconventional Conditions: Reagents, Reactors, and Modi Operandi, *Chem. Mater.*, 2020, 4884–4919, DOI: 10.1021/acs.chemmater.9b04741, American Chemical Society.
3 A. Navrotsky, O. Trofyrnluk and A. A. Levchenko, Thermochemistry of Microporous and Mesoporous Materials, *Chem. Rev.*, 2009, 3885–3902, DOI: 10.1021/cr800495t, American Chemical Society.
4 H. Koizumi and S. Uda, Theoretical and Practical Studies on Effects of External Electrostatic Electric Field on Nucleation and Growth Kinetics of Protein Crystals, *Prog. Cryst. Growth Charact. Mater.*, 2022, **68**(3), 100568, DOI: 10.1016/j.pcrysgrow.2022.100568.
5 M. Taleb, C. Didierjean, C. Jelsch, J. Mangeot, B. Capelle and A. Aubry, Crystallization of Proteins under an External Electric Field, *J. Cryst. Growth*, 1999, **200**(3–4), 575–582, DOI: 10.1016/S0022-0248(98)01409-2.
6 D. Hou and H. C. Chang, Ac Field Enhanced Protein Crystallization, *Appl. Phys. Lett.*, 2008, **92**(22), 223902, DOI: 10.1063/1.2938887.
7 Z. Hammadi and S. Veesler, New Approaches on Crystallization under Electric Fields, *Prog. Biophys. Mol. Biol.*, 2009, **101**(1–3), 38–44, DOI: 10.1016/j.pbiomolbio.2009.12.005.
8 M. I. Al-haq, E. Lebrasseur, H. Tsuchiya and T. Torii, Protein Crystallization under an Electric Field, *Crystallogr. Rev.*, 2007, **13**(1), 29–64, DOI: 10.1080/08893110701421463.
9 B. A. Frontana-Uribe and A. Moreno, On Electrochemically Assisted Protein Crystallization and Related Methods, in *Crystal Growth and Design*, American Chemical Society, 2008, vol. 8, pp. 4194–4199. DOI: 10.1021/cg800731p.
10 F. Li and R. Lakerveld, Electric-Field-Assisted Protein Crystallization in Continuous Flow, *Cryst. Growth Des.*, 2018, **18**(5), 2964–2971, DOI: 10.1021/acs.cgd.8b00095.
11 D. Ray, M. Madani, J. K. G. Dhont, F. Platten and K. Kang, The Effects of Electric Fields on Protein Phase Behavior and Protein Crystallization Kinetics, *J. Phys. Chem. Lett.*, 2024, **15**(31), 8108–8113, DOI: 10.1021/acs.jpclett.4c01744.
12 D. Ray, M. Madani, J. K. G. Dhont, F. Platten and K. Kang, Electric Field-Induced Control of Protein Crystal Morphology, *Soft Matter*, 2025, **21**(16), 3012–3021, DOI: 10.1039/D5SM00181A.
13 L. F. Alexander and N. Radacsi, Application of Electric Fields for Controlling Crystallization, *CrystEngComm*, 2019, **21**(34), 5014–5031, DOI: 10.1039/C9CE00755E.
14 D. Kashchiev, Nucleation in External Electric Field, *J. Cryst. Growth*, 1972, **13–14**(C), 128–130, DOI: 10.1016/0022-0248(72)90074-7.
15 R. Dhanasekaran and P. Ramasamy, Two-Dimensional Nucleation in the Presence of an Electric Field, *J. Cryst. Growth*, 1986, **79**(1–3), 993–996, DOI: 10.1016/0022-0248(86)90584-1.
16 K. V. Saban, J. Thomas, P. A. Varughese and G. Varghese, Thermodynamics of Crystal Nucleation in an External Electric Field, *Cryst. Res. Technol.*, 2002, **37**(11), 1188–1199, DOI: 10.1002/1521-4079(200211)37:11<1188::AID-CRAT1188>3.0.CO;2-5.
17 J. O. Isard, Calculation of the Influence of an Electric Field on the Free Energy of Formation of a Nucleus, *Philos. Mag.*, 1977, **35**(3), 817–819, DOI: 10.1080/14786437708236010.

18 W. W. Li, N. Radacsi, H. J. M. Kramer, A. E. D. M. van der Heijden and J. H. ter Horst, Solid Separation from a Mixed Suspension through Electric–Field–Enhanced Crystallization, *Angew. Chem., Int. Ed.*, 2016, **55**(52), 16088–16091, DOI: 10.1002/anie.201609832.

19 H. Koizumi, K. Fujiwara and S. Uda, Control of Nucleation Rate for Tetragonal Hen-Egg White Lysozyme Crystals by Application of an Electric Field with Variable Frequencies, *Cryst. Growth Des.*, 2009, **9**(5), 2420–2424, DOI: 10.1021/cg801315p.

20 G. Ivanushkin, I. Khalil, M. Torka Beydokhti, A. Bugaev, J. Bae, T. Donckels and M. Dusselier, The Pursuit of Framework Zinc Affirmation in Zincosilicate Zeolites: Clues from Conventional and Spectroscopic Characterization, *Microporous Mesoporous Mater.*, 2025, **387**, 113449, DOI: 10.1016/j.micromeso.2024.113449.

21 G. Ivanushkin, M. Torka Beydokhti, J. S. Martinez-Espin and M. Dusselier, Electro-Assisted Synthesis of Sn-Beta Zeolite Leads to Record Tin Incorporation and Superior Lewis Acid Catalysis, *Chem. Mater.*, 2023, **35**(23), 10216–10227, DOI: 10.1021/acs.chemmater.3c02465.

22 G. Ivanushkin and M. Dusselier, Engineering Lewis Acidity in Zeolite Catalysts by Electrochemical Release of Heteroatoms during Synthesis, *Chem. Mater.*, 2023, **35**(13), 5049–5058, DOI: 10.1021/acs.chemmater.3c00552.

23 N. Zhao, L. Zheng, Y. Sun, L. Zhang, Q. Qing, S. Liu, Z. Wang, X. Xiong, X. Wang and Y. Lu, Accelerated Crystallization of Zeolites under Ambient Conditions via Microplasma Electrochemistry, *Small Methods*, 2025, **9**(8), 2500404, DOI: 10.1002/smtd.202500404.

24 A. Huang and W. Yang, Hydrothermal Synthesis of Uniform and Dense NaA Zeolite Membrane in the Electric Field, *Microporous Mesoporous Mater.*, 2007, **102**(1–3), 58–69, DOI: 10.1016/j.micromeso.2006.12.005.

25 T. Yu, Y. Liu, W. Chu, Y. Liu, R. Cai and W. Yang, Insights into the Interplay between Electric Fields and Microstructures of AEL Films under Ionothermal Conditions, *Chem. Commun.*, 2017, **53**(11), 1836–1839, DOI: 10.1039/C6CC10021J.

26 T. Yu, W. Chu, R. Cai, Y. Liu and W. Yang, In Situ Electrochemical Synthesis of Oriented and Defect–Free AEL Molecular–Sieve Films Using Ionic Liquids, *Angew. Chem., Int. Ed.*, 2015, **54**(44), 13032–13035, DOI: 10.1002/anie.201506183.

27 A. Warty, A. Chen, D. T. Tran, H. Kraus, T. J. Woehl and D. Liu, Electrochemical Synthesis of Zeolite Coatings with Controlled Crystal Polymorphism and Self-Regulating Growth, *JACS Au*, 2024, **4**(12), 4769–4779, DOI: 10.1021/jacsau.4c00691.

28 K. Chen, S. H. Mousavi, Z. Yu, L. Zhang, Q. Gu, R. Q. Snurr, P. A. Webley, N. Sun and G. K. Li, Molecular Insight into the Electric Field Regulation of N2 and CH4 Adsorption in the Trapdoor ZSM-25 Zeolites, *ACS Appl. Mater. Interfaces*, 2024, **16**(38), 51129–51138, DOI: 10.1021/acsami.4c11059.

29 K. Chen, Z. Yu, S. H. Mousavi, R. Singh, Q. Gu, R. Q. Snurr, P. A. Webley and G. K. Li, Regulating Adsorption Performance of Zeolites by Pre-Activation in Electric Fields, *Nat. Commun.*, 2023, **14**(1), 5479, DOI: 10.1038/s41467-023-41227-4.

30 S. Zhou, Y. Wei, L. Li, Y. Duan, Q. Hou, L. Zhang, L. X. Ding, J. Xue, H. Wang and J. Caro, Paralyzed Membrane: Current-Driven Synthesis of a Metal-Organic Framework with Sharpened Propene/Propane Separation, *Sci. Adv.*, 2018, **4**(10), DOI: 10.1126/sciadv.aau1393.

31 A. Knebel, B. Geppert, K. Volgmann, D. I. Kolokolov, A. G. Stepanov, J. Twiefel, P. Heitjans, D. Volkmer and J. Caro, Defibrillation of Soft Porous Metal-Organic Frameworks with Electric Fields, *Science*, 2017, **358**(6361), 347–351, DOI: 10.1126/science.aal2456.

32 H. Ren and T. Wei, Electrochemical Synthesis Methods of Metal–Organic Frameworks and Their Environmental Analysis Applications: A Review, *ChemElectroChem*, 2022, **9**(13), e202200196, DOI: 10.1002/celc.202200196.

33 B. Yu and S. B. Khoo, Controllable Zeolite Films on Electrodes—Comparing Dc Voltage Electrophoretic Deposition and a Novel Pulsed Voltage Method, *Electrochem. Commun.*, 2002, **4**(10), 737–742, DOI: 10.1016/S1388-2481(02)00444-7.

34 W. Shan, Electrophoretic Deposition of Nanosized Zeolites in Non-Aqueous Medium and Its Application in Fabricating Thin Zeolite Membranes, *Microporous Mesoporous Mater.*, 2004, **69**(1–2), 35–42, DOI: 10.1016/j.micromeso.2004.01.003.

35 H. Negishi, K. Ueno and Y. Oumi, Effect of Electroosmotic Flow on the Electrophoretic Deposition of Zeolite Powder on a Porous Alumina Support, *ECS Trans.*, 2018, **82**(1), 13–18, DOI: 10.1149/08201.0013ecst.

36 L. Brabec, J. Plšek and M. Kočiřík, Electrophoretic Deposition of Zeolites Focused on Attendant Electrodecantation and Subsequent Growth of Electric Current, *ChemistrySelect*, 2019, **4**(11), 3185–3190, DOI: 10.1002/slct.201900510.

37 A. Walcarius, Recent Advances in Electrochemistry with Zeolitic Materials, *Curr. Opin. Electrochem.*, 2026, **56**(15), 101808, DOI: 10.1016/j.coelec.2025.101808.

38 S. Ghojavand, E. Dib and S. Mintova, Flexibility in Zeolites: Origin, Limits, and Evaluation, *Chem. Sci.*, 2023, **14**(44), 12430–12446, DOI: 10.1039/D3SC03934J.

39 M. Shen, F. Kong, W. Guo, Z. Zuo, C. Guo, L. Tong, S. Yin, L. Wang, S. Kawi, P. K. Chu and Y. Ding, Enhanced Direct Air Carbon Capture on NaX Zeolite by Electric-Field Enhanced Physical Adsorption and In Situ CO2 Synergistic Effects of Cold Plasma, *Adv. Funct. Mater.*, 2024, **34**(49), 2408922, DOI: 10.1002/adfm.202408922.

40 M. Ammam, Electrophoretic Deposition under Modulated Electric Fields: A Review, *RSC Adv.*, 2012, **2**(20), 7633, DOI: 10.1039/c2ra01342h.

41 G. Feng, P. Cheng, W. Yan, M. Borona, X. Li, J. H. Su, J. Wang, Y. Li, A. Corma, R. Xu and J. Yu, Accelerated Crystallization of Zeolites via Hydroxyl Free Radicals, *Science*, 2016, **351**(6278), 1188–1191, DOI: 10.1126/science.aaf1559.

42 Y. Hasegawa, C. Abe, M. Nishioka, K. Sato, T. Nagase and T. Hanaoka, Influence of Synthesis Gel Composition on Morphology, Composition, and Dehydration Performance of CHA-Type Zeolite Membranes, *J. Membr. Sci.*, 2010, **363**(1–2), 256–264, DOI: 10.1016/j.memsci.2010.07.040.

43 E.-P. Ng, D. Chateigner, T. Bein, V. Valtchev and S. Mintova, Capturing Ultrasmall EMT Zeolite from Template-Free Systems, *Science*, 2012, **335**(6064), 70–73, DOI: 10.1126/science.1214798.

44 X. Yang, E. Dib, Q. Lang, H. Guo, G. Fu, J. Wang, Q. Yi, H. Zhao and V. Valtchev, Silicalite-1 Formation in Acidic Medium: Synthesis Conditions and Physicochemical Properties, *Microporous Mesoporous Mater.*, 2022, **329**, 111537, DOI: 10.1016/j.micromeso.2021.111537.

45 M. Maldonado, M. D. Oleksiak, S. Chinta and J. D. Rimer, Controlling Crystal Polymorphism in Organic-Free Synthesis of Na-Zeolites, *J. Am. Chem. Soc.*, 2013, **135**(7), 2641–2652, DOI: 10.1021/ja3105939.

46 J. Devos, S. Robijns, C. Van Goethem, I. Khalil and M. Dusselier, Interzeolite Conversion and the Role of Aluminum: Toward Generic Principles of Acid Site Genesis and Distributions in ZSM-5 and SSZ-13, *Chem. Mater.*, 2021, **33**(7), 2516–2531, DOI: 10.1021/acs.chemmater.0c04832.

47 E. B. Clatworthy, M. Debost, N. Barrier, S. Gascoin, P. Boullay, A. Vicente, J.-P. Gilson, J.-P. Dath, N. Nesterenko and S. Mintova, Room-Temperature Synthesis of BPH Zeolite Nanosheets Free of Organic Template with Enhanced Stability for Gas Separations, *ACS Appl. Nano Mater.*, 2021, **4**(1), 24–28, DOI: 10.1021/acsanm.0c02925.

48 M. B. Park, S. H. Ahn, C. P. Nicholas, G. J. Lewis and S. B. Hong, Charge Density Mismatch Synthesis of Zeolite Beta in the Presence of Tetraethylammonium, Tetramethylammonium, and Sodium Ions: Influence of Tetraethylammonium Decomposition, *Microporous Mesoporous Mater.*, 2017, **240**, 159–168, DOI: 10.1016/j.micromeso.2016.11.013.

49 Y. Huang, M. Li, C. Shi, Z. Liu and B. Ren, Synthesis of Ultra-Small NaA Zeolite Nanocrystals at near Room Temperature, *J. Porous Mater.*, 2023, **30**(4), 1143–1147, DOI: 10.1007/s10934-022-01402-2.

50 Y. Liang, A. J. Jacobson and J. D. Rimer, Strontium Ions Function as Both an Accelerant and Structure-Directing Agent of Chabazite Crystallization, *ACS Mater. Lett.*, 2021, **3**(2), 187–192, DOI: 10.1021/acsmaterialslett.0c00460.

51 W. Fan, S. Shirato, F. Gao, M. Ogura and T. Okubo, Phase Selection of FAU and LTA Zeolites by Controlling Synthesis Parameters, *Microporous Mesoporous Mater.*, 2006, **89**(1–3), 227–234, DOI: 10.1016/j.micromeso.2005.11.001.

52 W. M. Meier and M. Groner, Zeolite Structure Type EAB: Crystal Structure and Mechanism for the Topotactic Transformation of the Na, TMA Form, *J. Solid State Chem.*, 1981, **37**(2), 204–218, DOI: 10.1016/0022-4596(81)90086-4.

53 J. Devos, M. A. Shah and M. Dusselier, On the Key Role of Aluminium and Other Heteroatoms during Interzeolite Conversion Synthesis, *RSC Adv.*, 2021, **11**(42), 26188–26210, DOI: 10.1039/D1RA02887A.

54 A. Javdani, J. Bae, G. Ivanushkin and M. Dusselier, Dual Organic Structure-Directing Agents in Zeolite Synthesis: Cooperation or Competition?, *Mater. Horiz.*, 2025, **12**(13), 4496–4509, DOI: 10.1039/D5MH00235D.

55 S. Seo, N. H. Ahn, J. H. Lee, L. M. Knight, J. G. Moscoso, W. A. Sinkler, S. Prabhakar, C. P. Nicholas, S. B. Hong and G. J. Lewis, Combined Alkali-Organoammonium Structure Direction of High-Charge-Density Heteroatom-Containing Aluminophosphate Molecular Sieves, *Angew. Chem., Int. Ed.*, 2019, **58**(27), 9032–9037, DOI: 10.1002/anie.201902623.

56 M. B. Park, D. Jo, H. C. Jeon, C. P. Nicholas, G. J. Lewis and S. B. Hong, Zeolite Synthesis from a Charge Density Perspective: The Charge Density Mismatch Synthesis of UZM-5 and UZM-9, *Chem. Mater.*, 2014, **26**(23), 6684–6694, DOI: 10.1021/cm501919d.

57 W. M. Saslow, The Electric Field, in *Electricity, Magnetism, and Light*, Elsevier, 2002, pp. 108–144. DOI: 10.1016/B978-012619455-5.50003-6.

58 Fundamentals of Electric Fields, in *Electromagnetics Explained*, ed. R. Schmitt, Elsevier, 2002, pp. 25–49, DOI: 10.1016/b978-075067403-4/50003-3.

59 J. Kim, S. A. Guelcher, S. Garoff and J. L. Anderson, Two-Particle Dynamics on an Electrode in Ac Electric Fields, *Adv. Colloid Interface Sci.*, 2002, **96**(1–3), 131–142, DOI: 10.1016/S0001-8686(01)00078-1.

60 S. Mintova, N. H. Olson, V. Valtchev and T. Bein, Mechanism of Zeolite a Nanocrystal Growth from Colloids at Room Temperature, *Science*, 1999, **283**(5404), 958–960, DOI: 10.1126/science.283.5404.958.

61 V. P. Valtchev and K. N. Bozhilov, Evidences for Zeolite Nucleation at the Solid-Liquid Interface of Gel Cavities, *J. Am. Chem. Soc.*, 2005, **127**(46), 16171–16177, DOI: 10.1021/ja0546267.

62 M. D. Oleksiak, J. A. Soltis, M. T. Conato, R. L. Penn and J. D. Rimer, Nucleation of FAU and LTA Zeolites from Heterogeneous Aluminosilicate Precursors, *Chem. Mater.*, 2016, **28**(14), 4906–4916, DOI: 10.1021/acs.chemmater.6b01000.

63 L. Hu, S. Xie, Q. Wang, S. Liu and L. Xu, Phase Selection Controlled by Sodium Ions in the Synthesis of FAU/LTA Composite Zeolite, *Sci. Technol. Adv. Mater.*, 2009, **10**(1), 015001, DOI: 10.1088/1468-6996/10/1/015001.

64 K. Adrjanowicz and R. Richert, *Control of Crystallization Pathways by Electric Fields*, Springer, Cham, 2020, pp 149–167. DOI: 10.1007/978-3-030-56186-4_6.

65 K. Kang and J. K. G. Dhont, Electric-Field Induced Transitions in Suspensions of Charged Colloidal Rods, *Soft Matter*, 2010, **6**(2), 273–286, DOI: 10.1039/B910046F.

66 R. Moreno, Colloidal Processing of Ceramics and Composites, *Adv. Appl. Ceram.*, 2012, **111**(5–6), 246–253, DOI: 10.1179/1743676111Y.0000000075.

67 P. Kurzweil, Electrochemical Double-Layer Capacitors, in *Electrochemical Energy Storage for Renewable Sources and Grid Balancing*, Elsevier, 2015, pp. 345–407. DOI: 10.1016/B978-0-444-62616-5.00019-X.

68 J. W. Lee, A. Mani and J. A. Templeton, Atomistic and Molecular Effects in Electric Double Layers at High Surface Charges, *Langmuir*, 2015, **31**(27), 7496–7502, DOI: 10.1021/acs.langmuir.5b00215.

69 P. Gaddam and W. Ducker, Electrostatic Screening Length in Concentrated Salt Solutions, *Langmuir*, 2019, **35**(17), 5719–5727, DOI: 10.1021/acs.langmuir.9b00375.

70 A. M. Smith, A. A. Lee and S. Perkin, The Electrostatic Screening Length in Concentrated Electrolytes Increases with Concentration, *J. Phys. Chem. Lett.*, 2016, **7**(12), 2157–2163, DOI: 10.1021/acs.jpclett.6b00867.

71 G. Loget, J. Roche and A. Kuhn, True Bulk Synthesis of Janus Objects by Bipolar Electrochemistry, *Adv. Mater.*, 2012, **24**(37), 5111–5116, DOI: 10.1002/adma.201201623.

72 S. Murad, The Role of External Electric Fields in Enhancing Ion Mobility, Drift Velocity, and Drift–Diffusion Rates in Aqueous Electrolyte Solutions, *J. Chem. Phys.*, 2011, **134**(11), 114504, DOI: 10.1063/1.3565478.